PERGAMON

Planetary and Space Science 49 (2001) 319–326

Planetary and Space Science

www.elsevier.nl/locate/planspasci

Satellite sputtering in Saturn's magnetosphere

S. Jurac[a,b,*], R.E. Johnson[b], J.D. Richardson[a], C. Paranicas[d]

[a] *Massachusetts Institute of Technology, MIT 37-662b, Cambridge, MA 02139, USA*
[b] *University of Virginia, Engineering Physics, Thornton Hall 103, Cahrlottesville, VA, 22903, USA*
[d] *Applied Physics Laboratory, Johns Hopkins Road, Laurel, MD 20723, USA*

Received 13 December 1999; received in revised form 10 August 2000; accepted 24 August 2000

Abstract

The heavy ion plasma and energetic particles continuously sputter the surfaces of the icy satellites embedded in the inner Saturnian magnetosphere. We evaluate satellite sputtering and compare the resulting H_2O source distribution with the source distribution expected for the OH cloud recently observed by Hubble Space Telescope. At each satellite we combine, for the first time, the data from the Plasma Science (PLS) and Low Energy Charged-Particle (LECP) instruments from Voyager 1 and 2, unifying them into a single plasma distribution function. Based on the calculated satellite sources, we conclude that sputtering of the satellite surfaces cannot produce the observed OH cloud and that a large additional source in the inner magnetosphere is needed to fully explain the HST observations.

1. Introduction

It has been proposed that the trapped plasma ions in Saturn's magnetosphere are derived from the surfaces of the icy satellites which orbit within the magnetosphere (Cheng et al., 1982; Eviatar and Richardson, 1992; Johnson et al., 1989). These moons are exposed to energetic ion bombardment which produces an ambient gas by a process called 'sputtering' (e.g., Johnson, 1990, 1998). The sputtered water molecules and their decomposition products are ionized by the plasma electrons and UV photons, and thus contribute to the local plasma density. Contrary to expectations, the direct observation of the extended neutral OH cloud by Shemansky et al. (1993) and Hall et al. (1996) suggested that this sputtering process might not be the dominant source of plasma. The density of OH, which is formed from dissociation of the ejected H_2O molecules, was too large to be accounted for by the present estimates of the icy satellite sputtering rates. The data initially used by Johnson and coworkers to describe the neutral cloud produced by sputtering of the icy satellites and the E-ring grains were re-evaluated (Johnson et al., 1989; Shi et al., 1995) and the sputtering sources revised upward. A new 2-D model for the neutral cloud, based on HST measurements of neutral OH (Richardson et al., 1998), showed an order of magnitude gap between the neutral source required and the sputter-induced production rate.

The modeling of the OH and plasma observations (e.g., Richardson et al., 1998) also confirmed that the ion residence times are relatively short so that local sources can dominate the local plasma density (e.g., Shemansky et al., 1993; Shemansky and Hall, 1992). Therefore, in some regions of the torus, the plasma density may be dominated by a satellite or a ring source. If this is the case, the instruments on CASSINI can be used to help determine satellite surface composition (Johnson and Sittler, 1990). In order to examine this possibility, and to further improve the sputtering rate calculations, we re-examine the satellite sputtering rates considering certain aspects of the process in more detail. Since the sputtering of small grains differs significantly from that of large objects, we re-evaluate the E-ring grains' contribution to plasma/neutral sources in a separate paper (Jurac et al., 2001).

We first describe the sputtering of the icy satellites and give results for the energetic ions, based on an extrapolation of the sputtering measurements using a Monte Carlo transport code (Jurac et al., 1998, 2001). We review the Voyager data for O ion fluxes at the icy satellites, including up-to-date corrections to inferred densities. The gap in the measured plasma fluxes between the Voyager PLS instrument (with energy range 10–5950 eV) and the

* Correspondence address: MIT 37-662b, Cambridge, Ma 02139, USA. Tel.: +1-617-452-2841.

E-mail addresses: jurac@space.mit.edu (S. Jurac), rej@virginia.edu (R.E. Johnson), jdr@space.mit.edu (J.D. Richardson), chris.paranicas@jhuapl.edu (C. Paranicas).

0032-0633/01/$ - see front matter
PII: S0032-0633(00)00153-7

LECP detector (which measured O ions in 100 keV–GeV energy range) is bridged using a modified kappa distribution function. This distribution function as proposed by Paranicas et al. (1999) was recently applied to combine Galileo plasma analyzer (PLS) and Energetic Particle Detector (EPD) data near Ganymede. We also consider the enhancement of the ion fluxes onto the satellite surfaces for those ions whose gyro-radii are comparable with the satellite radius. Including the correction for the ion gyro-radius effect becomes important at Saturn because, unlike at the Gallilean satellites, the inner Saturnian satellites have radii comparable to the gyroradii of those ions which dominate the sputtering. Therefore, we produce the first comprehensive plasma ion data set for modelling the irradiation effects at the icy satellites. We apply this data to the sputtering of these moons and find that the satellite sources are much too small to produce the dense region of the neutral and ion torii, especially near Enceladus.

2. Sputtering of an ice surface

There have been a number of compilations of the laboratory data for sputtering of low-temperature water ice (see Johnson, 1998; Baragiola et al., 2001 for reviews). A quantity of interest is the sputtering yield, the number of molecules ejected per incident ion, electron or photon. The yield primarily depends on the temperature of the ice, the ion energy and type and the angle of incidence. The ejecta are a mixture of H_2O, O_2 and H_2 with a small component of radicals. The maximum estimated temperatures on the icy Saturnian satellites are $\sim$ 100 K. Above this temperature, OH produced from the dissociation of H_2O by UV photons, electrons and fast ions can diffuse and the formation of other molecules becomes more common. Therefore, above $\sim$ 80–100 K the yields exhibit a temperature dependence (Johnson, 1990; Baragiola et al., 2001). In our model (Fig. 1) we consider only the temperature-independent data which we presume in the modeling primarily leads to the ejection of H_2O. The molecular species O_2 and H_2 show temperature-dependent yields and measurements exist only up to 5 keV (Bar-Nun et al., 1985). The plasma consists primarily of H^+, O^+, OH^+ and H_2O^+ (e.g., Richardson, 1998) with a small amount of O_2^+ and H_3O^+. The sputtering yield for incident H^+ is more than an order of magnitude lower than that for O^+ and, since the yields for OH^+ and H_2O^+ are close to that for O^+ at the same velocity, we consider here only sputtering by oxygen ions. If there is considerable pick-up of O_2^+ then significantly larger sputtering rates can result.

Fig. 1 shows a fit to the sputtering yields, $Y(E,\theta)$, summarized earlier (Johnson, 1990; Shi et al., 1995), for water ice vs. incident energy, E, for normal incidence, $\theta = 0$. The solid line represents the sputtering yield for incident O ions, calculated using a Monte Carlo binary collision code calibrated to laboratory data, as described in Jurac et al. (2001). This yield is used to calculate baseline sputtering source rates for each satellite. At non-normal incidence, the yields are larger since the ion's energy is deposited closer to the surface (e.g. Johnson, 1990). Shi et al. (1995) used an angular dependence in the yield based on that measured for light MeV ions (Brown et al., 1982, 1984), and assumed this dependence is not energy-dependent. For an isotropic incidence (i.e. integrated over all incident angles), that angular yield gave them a factor of 4 enhancement over the normal-incidence yield. Shi et al. (1995) applied this enhancement factor to the E-ring grains, assumed to have a non-porous surface, while no enhancement in the yield was applied to the satellites, whose surfaces are a porous regolith. Since a reliable model for the sputtering of a porous surface does not exist, here we give the energy-dependent yield for isotropic ions incident on a smooth surface, based on the Monte-Carlo simulation (Jurac et al., 2001). In Fig. 2, we plot the yield for an isotropic incidence at a given energy, $\langle Y(E,\theta)\rangle_\theta$, normalized to the yield for $\theta = 0$, $Y(E,0)$, in Fig. 1. The corresponding isotropic-incidence

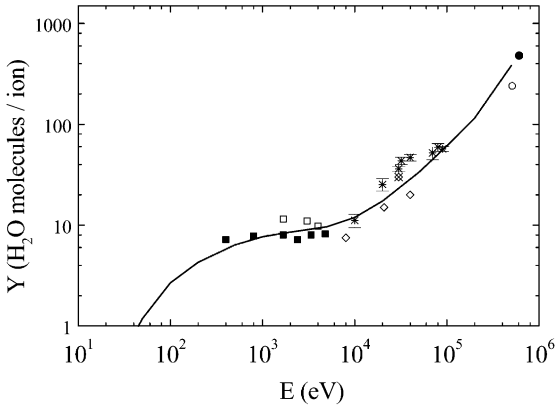

Fig. 1. Measured sputtering yield for water-ice at normal incidence for semi-infinite target versus incident O ion energy. Line indicates model given by Jurac et al. (1999), while symbols represent the compilation of laboratory measurements of the sputtering yield given by Shi et al. (1995).

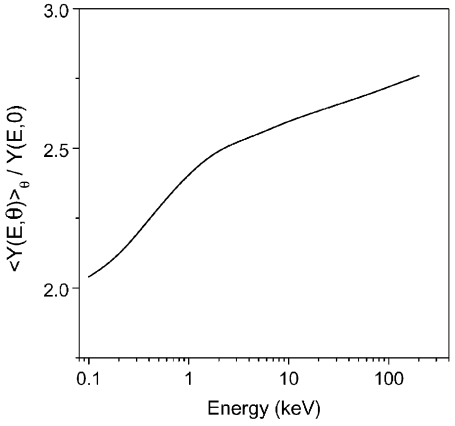

Fig. 2. Angle averaged sputtering yield on water-ice versus incident O ion energy normalized to the yield at normal incidence.

Table 1

Satellite	Sputter flux[a] (10^8 mol/cm^2/s) S_f	Effective satellite area[b] A_{eff}	Photo sputter flux[c] S_{ph}	Satellite source rate[d] (10^{26} molecules/s) $(S_f A_{eff} + S_{ph})4\pi S^2$	Escape fraction[e]	Angular enhancement[f]
Mimas	15.9	1.5	0.42	0.12	0.99	2.4
Enceladus	7.5	1.5	0.42	0.09	0.98	2.3
Tethys						
Low	6.6	1.5	0.42	0.35	0.95	2.4
High	7.6	1.5	0.42	0.41	0.95	2.4
Dione						
Low	3.9	1.5	0.42	0.25	0.9	2.4
High	6.5	1.5	0.42	0.40	0.9	2.4
Total						
Low				0.81		
High				1.03		

[a]H_2O sputter flux from an unit satellite area by O^+ ions. O_2 sputter flux estimates: 3.2 (Mimas), 2.2 (Enceladus), 2–2.3 (Tethys), 1.3–1.4 (Dione), with no angular enhancement.

[b]Effective satellite surface area enhancement due to the ion gyro-motion estimated by Shi et al. (1995) based on Pospieszalska and Johnson (1989) Monte-Carlo simulation.

[c]Averaged photo-sputtered flux from Shi et al. (1995) ignoring the enhancement for non-normal incidence due to porous satellite surface.

[d]Total satellite source rates $(S_f A_{eff} + S_{ph})4\pi S^2$ with S being the satellite's radius.

[e]Escape fractions from satellite surfaces, fraction of ejected H_2O molecules able to overcome satellites gravity, based on measured energy distribution of sputtered particles (Riemann et al., 1984) given by Johnson (1990).

[f]Angular enhancement for isotropic incidence for smooth surface (Jurac et al., 2001) averaged over the plasma distribution at each satellite. This factor was ignored here, assuming porous satellite surfaces.

enhancement factors, averaged over the plasma ion energy spectra, $\langle Y(E,\theta)\rangle_{E,\theta}/\langle Y(E,0)\rangle_E$ at each satellite, are given in Table 1.

A final quantity of interest is the energy distribution of the sputter ejecta. These distributions were measured for sputtering of ice for only a few incident ion types and energies (Riemann et al., 1984; Brown et al., 1984; Haring et al., 1984). In a nearly collisionless atmosphere, like that expected at the icy Saturnian satellites, the molecules sputtered from the surface form an exospheric gas. Molecules with an energy greater than the escape energy, escape from satellites and populate the local neutral cloud. The measured sputtered molecule velocity distributions can also be used to estimate the spatial extent of the neutral cloud. Earlier work calculated the mean speed of the H_2O molecules ejected into the neutral cloud (e.g., Johnson, 1990). These are smaller than the orbit speed but act to give a distribution out of the plane described by a 'scale height' and a mean width as discussed by Johnson et al. (1989). Based on the measured energy distributions (Johnson, 1990), the calculated escape fractions are also given in Table 1 for each satellite.

The above description of the yield is applicable to a laboratory surface. Such surfaces are irregular and slightly porous, but probably differ considerably from the icy satellite surfaces. The latter are assumed to resemble the surface of the Earth's Moon. Due to micrometeoroid impact, which shatters the surface, a vapor, fragments and 'pits' are formed. This produces a regolith, a porous surface composed of ~ 100 μm grains. Based on analysis of the satellite reflectance data (e.g., Clark et al., 1984), it has been suggested that the surfaces might have high values of porosity. Other interpretations of those data may be possible since the ion irradiation process itself determines the micro-scale surface structure. For instance, the irradiation can produce surface structure (Johnson et al., 1984) and voids which affect the reflectance (e.g., Johnson and Jesser, 1997). This effect has not been accounted for in calculating the porosity, but, of course, is 'included' in the measured yields.

Hapke and Cassidy (1978) studied the sputtering of a porous regolith in reference to the lunar surface. They showed that the porosity acts to reduce the sputtering yield from that for a refractory laboratory surface due to shadowing and due to the sticking of ejecta from one grain onto another. Recently, Smith and Kay (1997) showed that sticking occurs with near unit efficiency for surface temperatures and ejecta energies appropriate to the sputtering of ice. With such an assumption, Hapke (1989) estimated that the effective surfaces yields for a refractory material are an order of magnitude smaller than the laboratory data, whereas Johnson et al. (1989) calculated a more modest reduction for ices. The size of the reduction depends on the incident angle dependence of the yield and the angular dependence of the ejecta. Assuming that the satellite surfaces are much more porous than an irradiated laboratory sample, we ignore the angular enhancement factor in Table 1, until better information is available on the satellite surface structure.

Based on O_2 yields measured by Bar-Nun et al. (1985) we also give rough estimates for O_2 sputter flux (Table 1). As their measurements show a temperature-dependent yield, we used 2.5 for O_2 yield between 0.1–2 keV and 6 for energies 2–10 keV, assuming the surface temperature of 85 K.

3. Plasma fluxes

Measurements of the ion plasma flux used here were carried out by the Voyager 1 and 2 spacecraft during their passes through the magnetosphere. Each Voyager spacecraft had a plasma instrument (PLS) with energy range from 10 to 5950 eV and a low-energy charged particle detector (LECP) which included measurements of oxygen ions from ~ 100 keV to a few MeV. While the PLS and LECP electron measurements were unified to form a single plasma distribution function (Maurice et al., 1996), no attempt has been made to connect PLS and LECP ion data. In an earlier sputtering calculation, Lanzerotti et al. (1983) fit a line through the LECP measurements and extended it down to 6 keV, assuming only the presence of an H^+ population. Shi et al. (1995) gave lower limits to the sputtering rates using a 'flat' extrapolation from the lowest measured LECP energy channel down to the PLS data. Although the ions in the PLS energy range dominate the plasma density, the energetic ions (5–100 keV) play a central role in the sputtering, since the sputtering yield increases substantially with energy (Fig. 1). Therefore, putting these two Voyager data sets together gives the best estimate of the sputtering to date. We refer to the simultaneous fit of the PLS and LECP data as the 'O^+ distribution'.

For the LECP channels of interest here, individual ion contributions cannot be separately obtained. But based on the analysis of Krimings et al. (1983), it is reasonable to assume that inside Rhea's orbit LECP channels are dominated by O^+. Additionally, asymmetries in the LECP measurements between the V1/V2 inbound/outbound passes at the same L shell have been identified (see Krimings et al., 1983; Armstrong et al., 1983) as local time effects. Therefore, based on that asymmetry we give high and low estimates for the O^+ distribution and sputtering rates. It will be shown later that a difference of about a factor of 5 in the measured LECP fluxes translates into about a factor of two in uncertainty in the total sputtering rates. The Voyager 2 inbound/outbound LECP data used as a baseline for our O^+ fluxes are corrected for the electron contamination discovered at the time of the Voyager 2 encounter with Uranus (Mauk et al., 1987). This correction is important in Saturn's magnetosphere (Paranicas et al., 1997) and was not accounted for in previous sputtering calculations.

Richardson and Sittler (1990) used the PLS data to develop a model for the low-energy ions and electrons in Saturn's magnetosphere and calculated the plasma densities in the equatorial plane. Their equatorial densities and temperatures, which were further extrapolated inside the orbit of

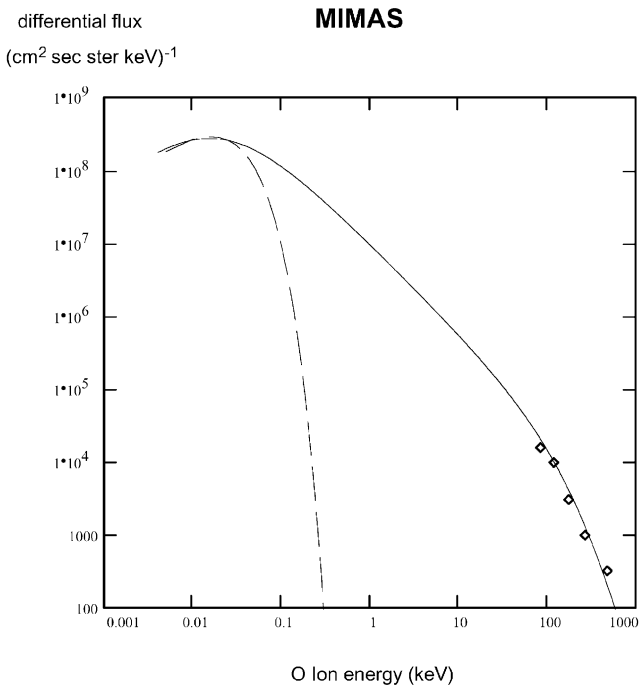

Fig. 3. Measured plasma flux (assumed O) by Voyager 2 LECP instrument (diamonds) near Mimas. Dashed line is the Maxwellian fit to the 'cold' O plasma component measured by Voyager PLS instrument, with temperature given by Richardson (1995). Solid line represents our fit with the Extened Kappa distribution given in Eq. (1).

Enceladus by Richardson (1995), are used to obtain a differential O^+ flux at each satellite. The ion data used in the model were derived by fitting the proton and heavy ion (taken to be O^+) components to Maxwellians. Although this technique characterizes the thermal plasma, it ignored the hot plasma component reported by Lazarus and McNutt (1983). We reanalyzed spectra near the satellites fitting an additional hot O^+ Maxwellian distribution to the data; although the distribution is likely non-Maxwellian, this method gives a rough characterization of the hot component. We then use this result to help bridge the energy 'gap' between the PLS and LECP measurements. The PLS O^+ ions 'cold' and 'hot' Maxwellians are used together with LECP measurements to constrain our plasma flux distribution.

The kappa function, used by Krimings et al. (1983) to fit LECP measurements, was found to be an inadequate representation of the full energy spectrum. Instead, we used the same function as Paranicas et al. (1999), who simultaneously fit the Galileo plasma and particle intensities with

$$j(E) = CE[kT(1+\gamma)+E]^{-(\gamma+1)}[1+(E/E_t)^{\beta}]^{-1}. \qquad (1)$$

This function has similarities to the kappa distribution: it reduces to a Maxwellian at low energy, a power law at intermediate energies and another power law at high energies. The resulting distributions for each of the satellites are given in Figs. 3–6. Fig. 6 shows the measured fluxes and obtained O^+ distribution at Dione. The 'cold' Maxwellian flux corresponding to the O^+ density in the equatorial plane given

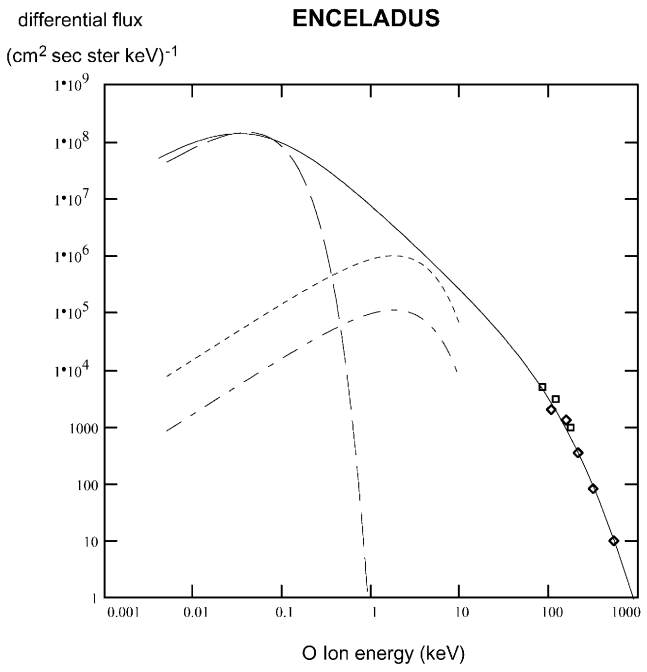

Fig. 4. Measured plasma flux (assumed O) near Enceladus by Voyager 1 (diamonds) and Voyager 2 (squares) LECP instrument and Maxwellian fits to the 'cold' (dash) and 'hot' (dash-dot) plasma components measured by Voyager 1 PLS instrument. The 'hot' component extrapolated to the equatorial plane is given as a dotted line. Solid line represents our fit connecting PLS and LECP measurements.

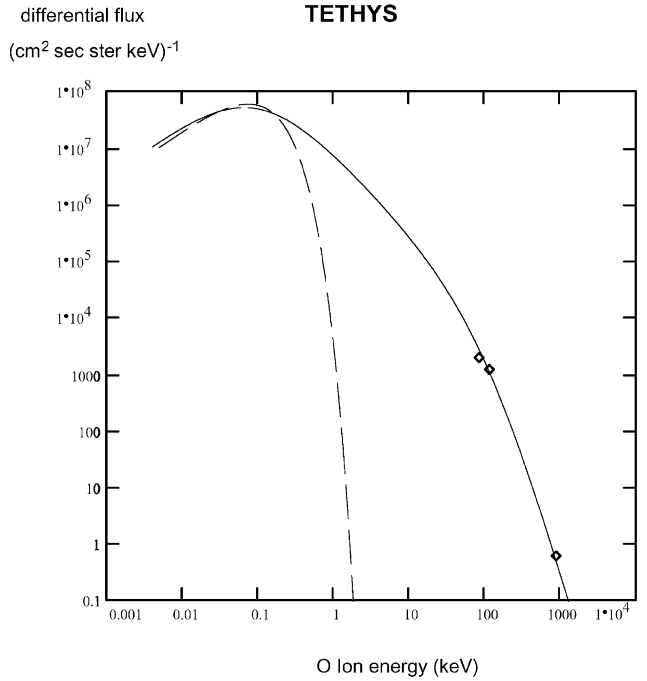

Fig. 5. Measured plasma flux near Tethys by Voyager 2 LECP instrument (diamonds). Dashed line is Maxwellian fit to the 'cold' plasma component based on PLS instrument, with temperature given by Richardson (1995). Solid line is our fit with the Extended Kappa distribution.

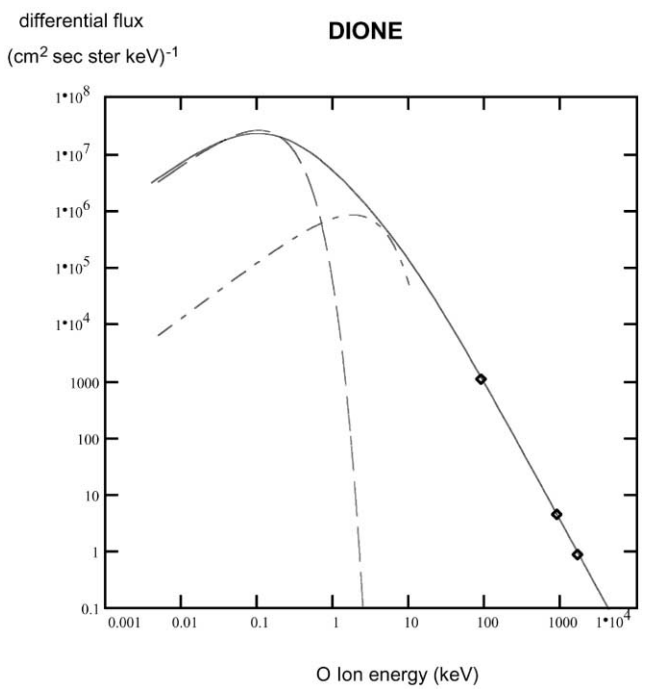

Fig. 6. Measured plasma flux near Dione by Voyager 2 LECP instrument (diamonds). Maxwellian fits to the 'cold' (dash) and 'hot' (dash-dot) plasma components based on Voyager 1 PLS instrument. Our fit with the Extended Kappa distribution is given as solid line.

by Richardson (1995) is plotted as a dashed line, the 'hot' Maxwellian fit to the upper PLS channels for V1 outbound is given as a dash-dot line, and LECP measured flux (assuming all O^+) as diamonds. Since V1 crossed the equatorial plane on the outbound trajectory at Dione, our 'hot' Maxwellian (dash-dot) represents equatorial values. The distribution function in Eq. (1), shown by the solid line in Fig. 6, is seen to be in a good agreement with the plasma data.

In Fig. 4, we show the combined plasma flux at Enceladus. At Enceladus V1, outbound was well above the equatorial plane and therefore measured lower intensities than it would near the magnetic equator. Consequently, the 'hot' flux (dash-dot) peaks at much lower intensity compared to 'cold' component (dash line), which was already extrapolated to the equatorial plane. If we use the same factor to scale the 'hot' component to the equator as for the 'cold' component found by Richardson and Sittler (1990), the 'hot' component is then given by the dotted line. Our fit (solid line) is then in reasonable agreement with the plasma data. Net fluxes at Mimas and Tethys based on the same extrapolation are given in Figs. 3 and 5. Generally, our fits to the plasma data fall between the simple extrapolations of Lanzerotti et al. (1983) and Shi et al. (1995).

The sputter flux from a unit satellite area is given by

$$F_s = \pi \int [Y(E) - 1]\Phi(E)\,\mathrm{d}E, \tag{2}$$

where $Y(E)$ represents the sputtering yield (Fig. 1), $\Phi(E)$ is the differential flux of incoming ions per steradian, and

$[Y(E)-1]$ in Eq. (2) is the yield reduced by the implanted incident particle. To calculate the satellite source rates we use an enhancement factor for the effective satellite surface due to the ion gyro-motion of 1.5, estimated by Shi et al. (1995) based on the Pospieszalska and Johnson (1989) Monte-Carlo simulation. We also include the photo-sputter flux given by Shi et al. (1995), which is small and not significant except at Dione (Table 1).

Voyager 1 LECP measurements are available for two satellites, Tethys and Dione, and the measured V1 LECP flux substantially exceeded those measured by V2 at the same dipole L shells (Krimings et al., 1983; Lanzerotti et al., 1983). To find uncertainties in the sputtering sources due to the different observed fluxes, we calculate the upper estimates to plasma distribution at Tethys and Dione. Because the correction for the electron contamination was not performed for V1 measurements, the rough high estimates are obtained by multiplying measured V2 LECP fluxes (diamonds in Figs. 3–5) by a factor of 3 at Tethys and 6 at Dione. This approximates the largest fluxes recorded by LECP instrument in the first LECP ion energy channel (PLO 1), based on measurements given by Lanzerotti et al. (1983). The estimates of the ion flux for Tethys and Dione together with the corresponding H_2O source rates are given in Table 1 ('high estimate').

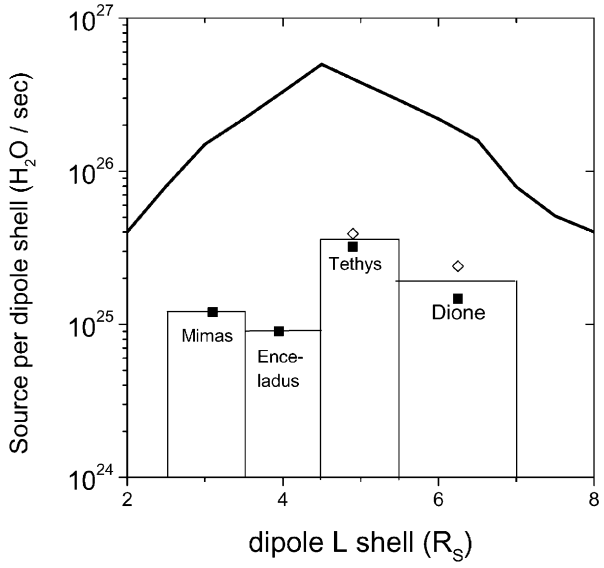

Fig. 7. Estimated sputtering H_2O source rates from satellites per dipole shell (in Saturn's radii). Required source rate from Richardson et al. (1998) plasma model is given as a thick solid line, while symbols represent our calculated satellite sources: low estimates are given as squares and high estimates as diamonds.

4. Results

Using the improved plasma flux distribution, at Enceladus we found about three times more H_2O produced than Shi et al. (1995), about the same at Tethys and about half as much at Dione. Our total estimated satellite source rate is between 0.8 and 1.0×10^{25} H_2O molecules/second. Thus, our upper limit for four inner satellites, is about the same as the lower limit of 1.2×10^{25} H_2O mol/s estimated by Shi et al. (1995), although the source distribution calculated here is quite different. The LECP fluxes used by Shi et al. (1995) are over-estimated above 100 keV, and underestimated below 100 keV due to a simple straight-line extrapolation. These authors also did not include Mimas in their total source rate, while we excluded Rhea since the LECP instrument response at Rhea may not be dominated by O ions (Krimings et al., 1983).

Fig. 7 shows our new satellite source rates per dipole L-shell and compares them to the supply rates calculated by Richardson et al. (1998). The supply rates were obtained using their plasma model and HST observations of the neutral OH cloud. Our source rates are multiplied by the escape fraction (a fraction of sputtered neutrals able to overcome a satellite's gravity, Table 1) given by Johnson (1990) based on the energy distribution of sputter ejecta measured by Riemann et al. (1984). The neutrals sputtered from Dione are spread out over a larger region because of the smaller gravitational force at a larger distance from Saturn. Scale heights and a mean width were estimated by Johnson et al. (1989). As indicated in Fig. 7, H_2O originating from Dione is spread over $1.5R_S$, while the rest of the satellites spread over about $1R_S$.

The satellite sources are much too small to produce the most dense region of the neutral and ion torii between Enceladus and Tethys. A large source of neutrals is needed near Enceladus to account for the measured OH densities in that region. Our estimated total satellite sources are at least an order of magnitude smaller than the source rate of 1.4×10^{27} H_2O/s required by Richardson et al. (1998), required to maintain the observed OH cloud. The addition of the previously estimated E-ring sputtering source (Shi et al., 1995) can account only for a small fraction (less than 10%) of this difference. Therefore, this calculation further exacerbates the problem of the 'missing' source of neutrals in Saturn's inner magnetosphere.

Since the electron temperatures have been extrapolated throughout this region, a possible explanation for this difference is that lifetimes for the water-like neutrals produced are longer than estimated (Richardson et al., 1998; Richardson, 1998) and, therefore, neutral/plasma sources required to maintain the observed OH cloud are smaller. However, it is doubtful this could fully account for the difference. An additional $\sim 25\%$ contribution of O_2 sputtered from ice could also be expected (Table 1) based on Bar-Nun et al. (1985) measurements. A band suggestive of O_3 has been observed in the surfaces of Rhea and Dione (Noll et al., 1998). The presence of O_3 in ice implies the presence of a precursor, such as O_2 or CO_2, which can cause the surface to be more volatile. Also, the exact composition of the satelitte surfaces is not known. The presence of more volatile species

trapped in the ice, such as CO_2 seen in the surfaces of the Jovian moons (McCord et al., 1998), or the presence of a fine grain ice on the surface, could enhance the calculated yields. Along these lines we have neglected $< 10\%$ effect not accounting for H ion sputtering. However, these additions are not expected to give an order of magnitude increase in the sputtering rate.

Another possibility for the difference between estimated sources and that required by Richardson et al. (1998) is that the E-ring may play a different role than presently thought. For instance, Hamilton and Burns (1994) proposed a self-sustaining E-ring model, in which small grains constantly bombard the icy satellites producing water vapor as well as fresh grains. Hyper-velocity ice grains (5 km/s) colliding with Enceladus might be partialy vaporized by impact (Ip, 1997), but the dominant modelling parameters are not well constrained at present.

Finally, the E-ring sputtering estimate in Shi et al. (1995) relies on the assumption that the E-ring consists of 1 μm grains only, i.e. uniform size distribution, which may be incorrect. The power-law size distribution is commonly expected from the disruptive collisional processes (Arakawa, 1999; Kato et al., 1995) and most of the grain population is then contained in smaller, submicron grains. That would result in much larger E-ring surface area, making it the dominant source of neutrals. This topic is pursued in detail in a subsequent paper (Jurac et al., 2001).

Acknowledgements

This work was supported by the Origins and the Geology and Geophysics programs of NASA at UVA, NSF Astronomy program at UVA and by NASA Planetary Atmospheres grant NAGW 5-6129 at MIT.

References

Arakawa, M., 1999. Collisional distribution of ice fragments by high velocity impact. Icarus 142, 34–45.

Armstrong, T.P., Paonessa, M.T., Bell II, E.V., 1983. Voyager observations of saturnian ion and electron phase space densities. J. Geophys. Res. 88, 8893–8904.

Baragiola, R.A., Vidal, R., Shi, M., Svendsen, W., Schou, J., Bahr, D., 2001. Sputtering of ices. Scanning Microscopy, submitted for publication.

Bar-Nun, A., Herman, G., Melker, Yu., 1985. Ejection of H_2O O_2 H_2 and H from water. ice by 0.5–6 keV H+ and Ne+ ion bombardement. Surf. Sci. 150, 143–156.

Brown, W.L., Augustyniak, W.M., Marcantonio, K.J., Simmons, E., Boring, J.W., Johnson, R.E., Riemann, C.T., 1984. Electronic sputtering of low temperature molecular solids. Nucl. Instr. and Meth. B 1, 307–314.

Brown, W.L., Augustyniak, W.M., Simmons, E., Marcantonio, K.J., Lanzerotti, L.J., Johnson, R.E., Boring, J.W., Riemann, C.T., Foti, G., Pirronello, V., 1982. Erosion and molecular formation in condensed gas films by electronic energy loss of fast ions. Nucl. Instr. and Meth. 198, 1–8.

Cheng, A.F., Lanzerotti, L.J., Pirronello, V., 1982. Charged particle sputtering of ice surfaces in Saturn's magnetosphere. J. Geophys. Res. 87, 4567–4570.

Clark, R.N., Brown, R.H., Owensby, P.D., Fanale, F.D., 1984. Saturn's satellites: near-infrared spectrophotometry (0.65–2.5 μm) of the leading and trailing sides and compositional information. Icarus 5, 265–281.

Eviatar, A., Richardson, J.D., 1992. Thermal plasma in the kronian magnetosphere. Ann. Geophys. Res. 10 (7), 511–518.

Hall, D.T., Feldman, P.D., Holberg, J.B., McGrath, M.A., 1996. Florescent hydroxyl emissions from Saturn's ring atmosphere. Science 272, 516–518.

Hamilton, D.P., Burns, J.A., 1994. Origin of Saturn's E-ring: self sustained, naturally. Science 264, 550–553.

Hapke, B.W., Cassidy, W.A., 1978. Is the moon really as smooth as a billiard ball/remarks concerning recent models of sputtering on the lunar surface. Geophys. Res. Lett. 5, 297–300.

Hapke, B., 1989. The surface of Io — a new model. Icarus 79, 56–74.

Haring, R.A., Pedrys, R., Oostra, D.J., Haring, A., de Vries, A.E., 1984. Reactive sputtering of simple condensed gases by keV ions III: kinetic energy distribution. Nucl. Instr. and Meth. B 5, 483–488.

Ip, W.-H., 1997. On neutral cloud distributions in the Saturnian magnetosphere. Icarus 126, 42–57.

Johnson, R.E., 1990. Energetic Charged-Particle Interactions with Atmospheres and Surfaces. Springer, Berlin.

Johnson, R.E., 1998. Sputtering and desorption form icy surfaces. In: Schmitt, B., deBergh, C. (Eds.), Solar System Ices. Kluwer, Netherlands, pp. 303–334.

Johnson, R.E., Jesser, W.A., 1997. O_2/O_3 micro atmospheres in the surface of Ganymede. Astrophys. J. Lett. 480, L79–L82.

Johnson, R.E., Lanzerotti, L.J., Brown, W.L., 1984. Sputtering processes: erosion and chemical change. Adv. Space Res. 4, 41–51.

Johnson, R.E., Pospieszalska, M.K., Sittler, E.C., Cheng, A.F., Lanzerotti, L.J., Sievka, E.M., 1989. The neutral cloud and heavy ion inner torus at Saturn. Icarus 77, 311–329.

Johnson, R.E., Sittler Jr., E.C., 1990. Sputter-produced plasma as a measure of satellite surface composition: The CASSINI mission. Geophys. Res. Lett. 17, 1629–1632.

Jurac, S., Johnson, R.E., Donn, B., 1998. Monte-Carlo calculations of the sputtering of grains: enhanced sputtering of small grains. Astrophys. J. 503, 247–252.

Jurac, S., Johnson, R.E., Richardson, J.D., 2001. Saturn's E ring and production of neutral torus. Icarus, in press.

Kato, M., Iijima, Y., Arakawa, M., Okimura, Y., Fujimura, A., Maeno, N., Mizutani, H., 1995. Ice on ice experiments. Icarus 113, 423–441.

Krimings, S.M., Carbary, J.F., Keath, E.P., Armstrong, T.P., Lanzerotti, L.J., Gloeckler, G., 1983. General characteristic of hot plasma and energetic particles in the Saturnian magnetosphere: results from the Voyager spacecraft. J. Geophys. Res. 88, 8871–8892.

Lanzerotti, L.J., Maclennan, C.G., Brown, W.L., Johnson, R.E., Barton, L.A., Riemann, C.T., Garrett, J.W., Boring, J.W., 1983. Implication of Voyager data for energetic ion erosion of the icy satellites of Saturn. J. Geophys. Res. 88, 8765–8770.

Lazarus, A., McNutt Jr., R., 1983. Low-energy plasma ion observations in Saturn's magnetosphere. J. Geophys. Res. 88, 8831–8846.

Mauk, B.H., Krimings, S.M., Keath, E.P., Cheng, A.F., Armstrong, T.P., 1987. The hot plasma and radiation environment of the uranian magnetosphere. J. Geophys. Res. 92, 15,283–15,308.

Maurice, S., Sittler, E.C., Cooper, J.F., Mauk, B.H., Blanc, M., Selesnick, R.S., 1996. Comprehensive analysis of electron observations at Saturn: Voyager 1 and 2. J. Geophys. Res. 101 (A7), 15,211–15,226.

McCord, T.B. et al., 1998. Organics and other molecules in the surfaces of Ganymede and Calisto. Science 280, 1242–1245.

Noll, K.S., Rousch, T., Cruikshank, D., Johnson, R.E., 1998. Detection of ozone on Saturn's satellites Dione and Rhea. Science 388, 45–47.

Paranicas, C., Cheng, A.F., Mauk, B.H., Keath, E.F., Krimings, S.M., 1997. Evidence of a source of energetic ions at Saturn. J. Geophys. Res. 104, 17,459–17,472.

Paranicas, C., Paterson, W.R., Cheng, A.F., Mauk, B.H., McEntire, R.W., Frank, L.A., Williams, D.J., 1999. Energetic particle observed near Ganymede. J. Geophys. Res. 104, 17,459–17,467.

Pospieszalska, M.K., Johnson, R.E., 1989. Magnetospheric ion bombardement of satellites: Europa and Dione. Icarus 78, 1–13.

Richardson, J.D., 1995. An extended plasma model for Saturn. Geophys. Res. Lett. 22, 1177–1180.

Richardson, J.D., 1998. Thermal plasma and neutral gas in Saturn's magnetosphere. Rev. Geophys. 36, 501–524.

Richardson, J.D., Eviatar, A., McGrath, M.A., Vasyliunas, V.M., 1998. OH in Saturn's magnetosphere: observations and implications. J. Geophys. Res. 103, 20,245–20,255.

Richardson, J.D., Sittler Jr., E.C., 1990. A plasma density model for Saturn based on Voyager observations. J. Geophys. Res. 95, 12,019–12,031.

Riemann, C.T., Boring, J.W., Johnson, R.E., Garrett, J.W., Farmer, K.R., Brown, W.L., 1984. Ion-induced molecular ejection from D_2O ice. Surf. Sci. 147, 227–240.

Shemansky, D.E., Hall, D.T., 1992. The distribution of atomic hydrogen in the magnetosphere of Saturn. J. Geophys. Res. 97, 4143–4161.

Shemansky, D.E., Matherson, P., Hall, D.T., Hu, H.-Y., Tripp, T.M., 1993. Detection of the hydroxyl radical in the Saturn magnetosphere. Nature 363, 329–332.

Shi, M., Baragiola, R.A., Grosjean, D.E., Johnson, R.E., Jurac, S., Schou, J., 1995. Sputtering of water ice surfaces and the production of extended neutral atmospheres. J. Geophys. Res. 100, 26,387–26,395.

Smith, R.S., Kay, B.D., 1997. Absorption, desorption and crystallization kinetics in nanoscale water films. Recent Res. Dev. Phys. Chem. 1, 209–219.